Title: Environmental Signal Propagation in Non-stationary Systems: The Impact of Delta Advance on Terrestrial to Marine Information Transfer

Authors: Anjali M. Fernandes[1], Arvind Singh[2], Kyle M. Straub[3]

[1]Department of Earth and Environmental Sciences, Denison University, 100 West College Street, Granville, Ohio 43023, U. S. A.

[2]Department of Civil, Environmental and Construction Engineering, University of Central Florida, Orlando, Florida, 32816, U. S. A

[3]Department of Earth and Environmental Sciences, Tulane University, 101 Blessey Hall, St. Charles Ave. New Orleans, Louisiana, 70118, USA

Corresponding author: Dr. Anjali M. Fernandes, Email: anjali.fernandes@denison.edu

This is a non peer-reviewed pre-print submitted to EarthArXiv, and in review at Journal of Geophysical Research.

Environmental Signal Propagation in Non-stationary Systems: The Impact of Delta Advance on Terrestrial to Marine Information Transfer

Authors: Anjali M. Fernandes[1], Arvind Singh[2], Kyle M. Straub[3]

[1]Department of Earth and Environmental Sciences, Denison University, 100 West College Street, Granville, Ohio 43023, U. S. A.

[2]Department of Civil, Environmental and Construction Engineering, University of Central Florida, Orlando, Florida, 32816, U. S. A

[3]Department of Earth and Environmental Sciences, Tulane University, 101 Blessey Hall, St. Charles Ave. New Orleans, Louisiana, 70118, USA

Corresponding author: Dr. Anjali M. Fernandes, Email: anjali.fernandes@denison.edu

Keywords: Shelf margins, deltas, turbidity currents, submarine sedimentation, continental slopes, hyperpycnal flow, sediment gravity flows

Abstract

When interpreting environmental signals in the deep marine sedimentary archive, separating the record of local flow and sediment dynamics from that of the terrestrial transport system that feeds it can be challenging. We used a physical experiment to study the dynamics of flow and sedimentation on a prograding, hyperpycnal flow-dominated delta, shelf and submarine slope subject to slow rates of base-level rise (pseudo-subsidence). Our experiments are most relevant to shelf margins where sediment-rich deltaic systems can prograde towards the shelf edge under relatively mild rates of relative sea-level rise, e.g. recent millennia (~7 ky). Our results offer interesting insight into linked dynamics of terrestrial and submarine transport systems; they apply to timescales that range from days to millennia, and may be relevant to problems as diverse as delivery of dissolved and particulate anthropogenic pollutants to deep ocean ecosystems and terrestrial paleoenvironmental reconstructions from marine sedimentary records.

We asked 3 questions: (1) Are delta channel dynamics reflected in flow and sedimentation on the continental slope? (2) How effectively do shelf and slope systems transfer information from upstream? (3) How does delta growth and progradation to the shelf edge impact sedimentation on the continental slope?

We found that: (1) Changes in flow partitioning through delta-top channels and associated hyperpycnal plume dynamics are recorded in flow and sedimentation on the slope. Channelized delta-top flow resulted

in higher localized water discharge and sediment concentrations, and thick, fast-moving, and laterally continuous, turbidity currents on the slope; sheet flow on the delta top, on the other hand, produced thin, slow-moving and laterally discontinuous turbidity currents on the slope. (2) Patterns in flow and sedimentation correlate over longer distances on the advection-settling-dominated subaqueous continental slope than on the traction-dominated, transport-limited shelf and delta-top. (3) Delta progradation played an important role in defining the scales of depositional topography and sedimentation dynamics on the slope.

1. Introduction

Thick deposits on continental margins preserve the most complete record of past environmental states on Earth (National Research Council, 2010); however, interpretation of this record is fraught with uncertainty. Developing theory to parse environmental information from marine sedimentary records is essential for deep time reconstructions of climate, tectonics and surface processes (National Research Council, 2012) and for forecasting the impacts of environmental perturbation (e.g., climate change, pollution, land-use changes) on deep marine environments.

A challenge specific to the sedimentary records of submarine environments is the difficulty in separating the dynamics of the prograding delta and channel network from local dynamics. Observing these dynamics in real-time is challenging because (a) with few exceptions (e.g., Khripounoff et al., 2003; Xu et al., 2010; Hughes Clarke, 2016; Azpiroz-Zabala et al., 2017; Symons et al., 2017; Hage et al. 2019) no direct connections between terrestrial and submarine transport systems exist as deltas of the world are set far back on their continental shelves due to the current sea-level highstand, and (b) the autogenic timescales in question are on the order of hundreds or thousands of years. To fill this knowledge gap, we carried out an experiment to assess the impact of delta progradation on the linked dynamics of flow and sedimentation in terrestrial and submarine environments. We specifically focused on exploring the impact of shoreline position relative to the shelf edge on flow and sedimentation in subaerial and submarine environments.

The evolution of shelf margins is often reconstructed indirectly from the stratigraphic record, from which significant information is missing due to periods of erosion and/or hiatuses in deposition. The depositional record of shelf margin dynamics imaged in acoustic data (Sylvester et al., 2012; Swartz, 2019; Straub and Mohrig, 2006) or outcrops (Porebski and Steel, 2006; Dixon et al., 2012), while insightful, is static. Observations from physical (Straub, 2019; Kim et al., 2013) or numerical experiments

(Harris et al., 2016, 2020) can capture the kinematics of shelf margin evolution and thereby complement observations from static data-sets.

Harris et al. (2016, 2020) investigated the impact of greenhouse and icehouse sea-level oscillations on the volumes and extent of sedimentation on the slope. They used a numerical model, Dionysis (Granjeon, 1999), with a sediment diffusion algorithm that does not account for the autogenic variability in the transport system. This simplification proved profoundly insightful for broad comparisons between greenhouse and icehouse shelf margins but did not capture the rich autogenic variability observed on shorter timescales.

Kim et al. (2013) and Straub (2019) performed physical experiments to investigate linked shelf and slope systems with a delta prograding to a shelf edge. In their experiment, subaqueous sediment was transported as bedload, turbidity current formation was precluded, and the sub-aqueous slope primarily evolved through grain-flow processes. Straub (2019) used an experimental design in which hyperpycnal plumes exported sediment beyond the delta front. Kim et al. (2013), demonstrated that the delta's arrival at the shelf edge enhanced the volumes of sediment fluxed beyond the shelf edge. Incision of the deltaic feeder channel at the shelf edge caused it to "lock" in place. Reinforcing the findings of Kim et al. (2013), Straub (2019) observed that the arrival of the delta at the shelf edge marked a change in the organization and kinematics of the shelf transport system and resulted in an increase in the timeframe between delta channel avulsions.

Querying shelf margin evolution on longer timescales, Straub (2019) investigated the degree to which the magnitude and duration of sea-level cycles relative to autogenic length- and timescales can affect predictability in depositional locii of shelf margin systems. They found that the amplitude and timescale of sea-level cycles did not significantly influence the averaged volumes of sediment fluxed to the deep marine, but did appear to alter the predictability in the timing of sediment delivery to the deep marine. Sea-level cycles with larger scales relative to the autogenic scales of the sediment delivery tended to deliver the maximum amount of sediment to deep marine settings during lowstands, and cycles with smaller relative scales sometimes fluxed significantly larger volumes during highstands.

In the current work, we complement past efforts with a prograding experimental delta and shelf coupled to a subaqueous slope fed by hyperpycnal flows (Fig. 1A). Hyperpyncal plumes have been documented in a few rivers around the world, including the Huanghe river, China (Wright et al., 1990), the Salinas River, California (Johnson et al., 2001), and a suite of creek, called Foumara, in Italy (ref) and may constitute a direct link between rivers and the deep ocean. Turbid river plumes which evolve into turbidity currents must go through several transitions from normal river flow, through a fluvial backwater zone, a depth-limited plume and a plunging river plume before they can transform into turbidity currents (Fig. 1B; Akiyama and Stefan, 1984; Lamb et al., 2010). The backwater-influenced zone extends for some distance upstream of the shoreline where the river is influenced by the standing body of water in the basin (Chow, 1959; Henderson, 1966); the length of the backwater zone scales with the depth of the river within the normal flow zone divided by the gradient of the river in the normal flow zone. The depth-limited plume is the zone beyond the shoreline where the plume expands within the water column until it reaches a sufficient depth to plunge (Akiyama and Stefan, 1984). The plunging plume forms as the plume collapses and accelerates before it becomes a turbidity current.

Physical experiments produce spatial structure and kinematics that scale well, if imperfectly, to natural systems despite differences in spatiotemporal scales, material properties, and the number of active processes (Paola et al., 2009). They can offer insight into the evolution of natural landscapes over human and/or geological timescales and facilitate methodical exploration of the parameter space occupied by boundary conditions that influence natural systems (e.g., mass fluxes, base-level change). While the autogenic behavior of deltas and their response to allogenic perturbations have been explored with a substantial body of experimental work (e.g., Wang and Straub, 2009; Li et al., 2014; Heller et al., 2001; Hoyal and Sheets, 2009; Martin et al., 2009), experiments that couple terrestrial and marine systems are yet in their infancy.

Data and analyses presented herein specifically target the linked evolution of flow and deposition on shelf and slope. In particular, we investigate 1) the influence of delta channel network dynamics on flow and sedimentation on the continental slope, 2) the efficacy of shelf and slope systems, with intrinsically different sediment transport dynamics, in propagating environmental information downstream, and 3) the impact of shoreline proximity to the shelf edge on slope sedimentation. Applicable to significantly shorter geologic timescales than previous work, these experiments offer insight into shelf margin morphodynamics when relative sea-level rise-rates are small and deltas migrate towards the shelf edge. Applicable potential scenarios include: (1) recent geologic time, when deltas prograded towards the shelf edge under relatively small rates of sea-level rise that followed the phase of rapid sea-level rise associated with ice-sheet retreat, (2) rising limbs of greenhouse sea-level cycles, when sediment-rich deltaic systems could keep up with sea-level rise (e.g., Carvajal and Steel, 2006), and (3) modern systems where delta networks structures may enhance or limit pollutant delivery to the deep ocean.

2. Experiment Design and Data Collected

a. Basin configuration and experiment design

The experiment was performed under controlled and steady boundary conditions (i.e., fixed sea-level rise rate, sediment and water discharge) in Tulane's Deep-water Basin (TDWB), which is 6 m long, 5 m wide and 2.2 m deep (Fig. 1). The experiment surface consisted of a flat, submerged shelf and a subaqueous ramp. The flat shelf was 1.4 m wide in the stream-wise direction, 2.2 m wide in the cross stream direction; the ramp was 3.2 m long in the stream-wise direction and 2.2 m wide in the cross-stream direction, and had a slope of 5.7 degrees. Flow and sediment entered the basin by passing through a wire cage filled with gravel, which extracted momentum from the flow. Any flow that traveled off the edge of the subaqueous slope collected beneath a false floor and was extracted from the bottom of the basin, while fresh water was delivered into the basin at the top of the water column to maintain water elevation and to maintain the freshness of the ambient fluid. The mass balance of water in and out of the basin was calibrated and regulated by using an external, computer-controlled weir. Salt and water were mixed in a 2350L reservoir. From the reservoir, the fluid was pumped up to a constant head tank and then discharged into the basin under the influence of gravity. Sediment was added to the flow using a Schenk Accurate sediment feeder. During each incremental experimental run, the mixture of saline fluid and sediment was released into the basin, where it traveled across a flat shelf, leaving a fraction of its sediment load behind to build a delta. Flows plunged at the front of the delta to form a hyperpycnal plume that traveled across the subaqueous shelf and down the slope as a turbidity current (Fig. 2). In these experiments, shallow deltaic channels with relatively steep gradients did not develop a significant backwater zone.

b. Experimental Conditions

The total experimental run time was 26 hours. The ratio of water discharge to sediment discharge was 52:1, with water discharge being 0.17 L/s and sediment discharge being 0.0032 L/s. The sediment mixture contained 20% weight fine-grained sand (d_{10} = 50 μm; d_{50} = 70 μm; d_{90} = 200 μm) and 80% weight crushed silica flour (d_{10} = 3μm; d_{50} = 10 μm; d_{90} = 70 μm). A constant rate of sea-level rise equal to 3 mm/hour was applied and maintained to mimic uniform subsidence. $CaCl_2$ salt was added to the water to provide a 2% excess density relative to the freshwater in the basin. The salt in the fluid mimicked that component of the sediment load which behaves as wash load in natural systems. The pseudo-subsidence rate and the mixture of sediment, salt and water were selected to ensure there was sufficient coarse sediment in the flow to construct a delta that could (a) keep pace with the imposed sea-level rise rate, (b) consistently prograde towards the shelf edge, and (c) continuously flux a significant fraction of the supplied sediment past the shoreline as suspended load in hyperpycnal plumes. Each individual experimental run lasted for a duration of ten minutes. At the end of each 10-minute run, flow and sediment supply were turned off, and fresh water was circulated through the basin.

c. Data

Overhead photographs (Fig. 2) of the experimental surface during and after each 10-minute incremental flow were captured using an array of synchronized cameras; blue food dye was injected into the flow exactly 20 seconds before photographs were taken, allowing enough time for the dye front to travel partway through the experimental system. Photographs were used to map flow paths defined by blue food dye injected into the flow and to track surface changes that occurred every 10 minutes. At every 2-hour increment in experimental runtime, high resolution topographic maps were generated using a laser distancing system with 4mm horizontal resolution and 0.25 mm vertical resolution (Fig. 3A). During each 10-minute incremental flow, strike-oriented topographic transects of the sub-aqueous slope were collected at 2.5 m, 2 m, 3.5 m, 4 m, and 4.5 m from the inlet using a SONAR transducer with 4mm horizontal resolution and 0.25 mm vertical resolution). At the end of the 26-hour experiment, the deposit was sectioned and photographed (Fig. 4A).

3. Results

a. Source to sink sediment partitioning, stratigraphic architecture, and transport regimes

On a continental shelf margin with a delta that is distant from the shelf edge, sediment is partitioned to (a) the delta top, where it compensates for the effects of compactional or tectonic subsidence and sea-level rise, (b) the delta front, where it contributes to maintaining or advancing the shoreline during relative sea level rise, (c) the pro-delta, where it builds sub-aqueous mouth bars and modifies the shelf bathymetry and sub-aqueous accommodation space for future sedimentation. Accounting for 35% porosity, we calculated that roughly 40% of the supplied sediment was stored on the delta top and delta front (Fig 4). Neglecting fluid entrainment by the plunging plumes, we estimate that the hyperpycnal plumes that plunged at the delta front had initial sediment concentrations equal to roughly 1.35% and initial excess densities equal to roughly 4.1% at the shoreline. Approximately 10% of the supplied sediment was consistently removed from transport through deposition in the prodeltaic region (Fig. 4 A-D). Therefore, approximately 60% of the supplied sediment volume, carried downstream by turbidity currents, built the remainder of the sub-aqueous shelf and slope deposits. For the duration of the experiment, turbidity currents on the shelf and slope were depositional (no erosion was observed).

Accumulated shelf strata (Fig. 4 A, B), roughly 25 cm thick on the shelf, tapered from an average thickness of 25 cm on the upper slope at 2.5 m from the inlet to 0.2 cm at 4.5 m from the inlet, with cross-stream total stratal thicknesses being more spatially variable on the slope than on the shelf. Coarse grained deposits, identified by the red sand in the sediment mixture, were present in scour-based delta top channel fills, horizontal overbank strata and inclined delta foresets; sand-rich deposits were thickest in delta foresets and relatively thin in over bank deposits.

b. Delta size, shoreline morphology and flow patterns

During the experiment, the delta prograded across the flat shelf and sedimentation on the slope was fed by hyperpycnal plumes from delta channel mouths (Fig. 2). We used the orthorectified over-head photographs collected during each experimental flow to characterize flow patterns and delta shape during each experimental run. Shorelines were picked manually on each photograph and the distance of each shoreline pixel to the inlet was measured to compute the mean delta radius (Fig. 5A) and the variance in delta radius (Fig. 5B).

The photographs were converted to binary flow maps. Pixels on the subaerial delta were assigned a value of 1 if they were blue and a value of 0 if they were not. The ratio between the total number of blue pixels relative to the total number of delta top pixels was used to separate periods when flow was channelized from periods when sheet flow covered much of the delta-top (Fig. 2C).

During the first 8 hours of the experiment, the area of the delta-top was small and frequently inundated by sheet flow (Fig. 5C). At these early stages of delta growth, while flow was rarely channelized, the mean delta radius (Fig. 5A) and the variance in the radius (Fig. 5B) were small. When the delta-top area grew larger, flow alternated between sheet flow and channelized flow. While flow was channelized, mouth bars grew at the terminus of channels, became emergent and caused local progradation of the shoreline (See Hour 14 on Fig. 2 and Fig 3A and B). This increased shoreline rugosity and the variance in measured delta radius (Fig. 5A, B). The area inundated by sheet flow decreased as the experiment progressed (Fig. 2C). This occurred through delta-top aggradation and steepening, which is then followed by channel incision and localized shoreline progradation.

Channelized flow and sheet flow are associated with periods of sediment erosion and storage, respectively (Sheets et al., 2002; Kim et al., 2009; Powell et al., 2012). During periods of sediment erosion, downstream sediment flushing, and shoreline progradation, flow is primarily partitioned to a small number of channels. In this experiment, sediment is flushed through and deposited at the downstream termini of channels in mouth bars at the delta front, and on the shelf and slope. The increased length of channels reduces the longitudinal channel gradient (Kim et al., 2014). The resulting decrease in sediment transport capacity causes channel filling, lateral flow expansion and widespread inundation by sheet flow. Periods of inundation by sheet flow are tied to widespread deposition, shoreline retreat and a steepening of the longitudinal gradient. With this experiment, we are well placed to explore the impact of these autogenic storage and release cycles on hyperpycnal flows and marine sedimentation.

c. Linking flow patterns on shelf and slope

At cross-stream transects located at 1.5 m, 2 m, 2.5 m, 3 m, 3.5 m, 4 m, and 4.5 m from the inlet, we used binary flow maps to (a) identify sites along a transect that were visited by flow more frequently than others (Fig. 6A), (b) evaluate the spatial extent covered by subaerial flow or subaqueous turbidity currents at each transect (Fig. 6A, B) and evaluate relative abundance of laterally discontinuous flow versus laterally continuous sheet flow (Fig. 6C), and (c) compare flow patterns in proximal and distal areas to characterize the similarity between the former and the latter (Fig. 7A-C).

Flow patterns on the delta top varied along a spectrum from predominantly channelized flow that covered a small fraction of the delta surface (See Fig. 2, Hour 26) to predominantly sheet flow that covered much of the delta top. Channels with a clear topographic expression did not form on the subaqueous shelf and slope. Flow patterns varied between widespread and laterally continuous sheets of relatively thick flow (See Fig. 2, Hour 4) to laterally discontinuous “lanes” of thin flow often characterized by roll waves (See Fig. 2, Hour 19; Balmforth and Mandre, 2004).

Stacked binary data at each transect (Fig. 6A) were used to visualize the total number of times flow visited each point on the transect through time. Peaks indicate locations that have been visited by flow more often and troughs represent locations visited by flow less often, whereas the absence of clearly defined peaks and troughs indicate flow visited all locations across the transect in a relatively uniform manner. Contrasting patterns of flow on the shelf (i.e., weakly defined peaks) through distal slope (i.e., well-defined peaks) indicate that flow on the shelf visited all locations more uniformly than flow on the slope. Furthermore, at the distal slope transects, 3.5 - 4.5 m from the inlet (Fig. 6A), the relief between peaks and troughs in flow occurrence is more pronounced than at more proximal slope transects; this suggests that proximal slope transects were visited more uniformly by flow whereas turbidity currents tended to preferentially revisit some locations more than others at distal transects.

Distal slope transects were visited by flow less often than flow on the shelf, as indicated by the smaller flow occurrence values in distal transects at. This may be the result of (a) differences in flow dynamics, (b) sensitivity to topographic steering, and/or (c) an artifact of experimental design. For instance, expanding hyperpycnal plumes sometimes flowed off the edges of the sloping ramp before reaching distal transects, downstream dilution of turbidity currents sometimes caused currents to die before reaching distal transects, and the dye front in thin, slow currents did not reach the distal slope by the time the photographs were collected.

At each transect, we performed two simple calculations to further characterize flow patterns: (1) we integrated the number of blue pixels at each time-step and divided this value by the total number of pixels in the transect (Fig. 6B), and (2) we integrated the number of points at boundaries that defined the edges of flow along each transect at each time-step (Fig 6C). We used these two calculations to characterize the degree to which flow covered the experimental surface through time, as well as the degree of lateral continuity in flow. For example, a transect dominated by channelized subaerial flow or laterally discontinuous subaqueous turbidity currents show a relatively small fraction of the transect is occupied by flow in Figure 6B coupled with a greater number of flow edges in Figure 6C. Conversely, the experimental surface was covered by sheet flow if a large fraction of the transect is occupied by flow in Figure 6B and coupled with a small number of flow edges in Figure 6C.

On the shelf, we observe a temporal evolution from sheet flow to more laterally restricted delta-top flow at the transects at 1m, 1.5 m and 2 m from the inlet (Fig. 2, 6A, B, C). The transect on the uppermost slope (2.5 m from the inlet) showed little, if any, change in flow coverage or lateral restriction through time (Fig. 6B, C), and some locations were visited by flow more often than others (Fig. 6A). Farther downstream, at 3 m, 3.5 m, 4 m, and 4.5 m, flow coverage increased through time (Fig. 6B), with no discernible change in lateral discontinuity (Fig. 6C). At 3 m and 3.5 m from the inlet, a slight decrease in the degree of lateral discontinuity through time is observed (Fig. 6C); no consistent change in lateral discontinuity was observed at 4 m and 4.5 m from the inlet.

Observations of flow patterns on shelf and slope may be summarized as follows:

(a) From proximal shelf to distal slope, flow transitioned from dynamic to persistent, with flow visiting all locations along the transect more uniformly on the shelf and revisiting a few locations often on the distal slope.

(b) As the delta prograded, flow on the shelf to transitioned from predominantly sheet flow to predominantly channelized flow, and flow coverage on the slope to increase through time. Flow on the proximal slope became more laterally continuous over time, whereas flow on the distal slope did not .

d. Connecting flow patterns on shelf and slope

We investigated connections between autogenic changes in flow patterns (i.e., sheet flow to laterally restricted flow on the growing delta and slope. To do this, we first detrended the flow coverage data in Figure 6B at all 6 cross-stream transects. Next, we plotted the detrended flow coverage associated with every time-step at each transect to that at every transect downstream of it (Fig.7A).

Flow patterns on both the shelf and slope show the strongest similarity to flow patterns at the transect that is directly downstream, as indicated by the positive slope in the plots on the far left of each row of plots in Figure 7A. The best-fit linear slope in each case is steeper in the plots which compare locations on the slope than it is in plots that compare locations on the shelf (Fig. 7, A, B). Furthermore, the fit of the data is noticeably stronger between locations on the slope than between locations on the shelf; significant scatter is associated with data from shelf locations.

When transects at roughly 1 m apart are compared (all plots that are second from the left on each row in Figure 7), flow patterns on the slope are more similar than those on the shelf; we observe that the slope of the trendline is almost zero for locations on the shelf, but still positive and closer to 1 on the slope. The best-fit linear slope of the data decreases and the data scatter increases when the distances between transects increases (Fig. 7 B). The decrease in slope of the trendline is more pronounced on the shelf (see the first, second and third plots from the left in row 1 and 2 of Figure 7); it is less pronounced on the slope (see the first, second and third plots from the left in row 4 and 5 of Figure 7)

When data from locations on the shelf are plotted against locations on the slope, we observe that the slope of the trendline decreases from positive to negative when the distance between the transects being compared increases. When shelf locations are compared to locations immediately beyond the shelf edge (see column 3, rows 1 and 2 in Figure 7), the slopes of the trendline are very close to zero. The color-coded data-points in these plots suggest that, through time, the slope associated with smaller time increments fluctuated between positive and negative, indicative of fluctuation between similar and dissimilar flow patterns. When comparing locations on the shelf to locations on the continental slope, the slope of the trendlines becomes increasingly negative with distance between transects (see rows 1 and 2 in Figure 7). Flow patterns at distal slope transects display an inverse relationship with flow patterns on the shelf.

The scatter plots of flow on the shelf (1 m and 1.5 m), the shelf edge (2 m) and the uppermost slope (2.5 m) show temporally discrete subsets within the plotted data with positive and negative slopes, indicating that the compared locations oscillate between similar and dissimilar flow patterns, as shelf areas evolve from subaqueous to subaerial. Distal slope locations, on the other hand, display uniformly dissimilar flow patterns from those observed on the shelf (see Fig. 7, row 1).

Similarity in flow coverage, indicated by the positive linear slope of the cross-plotted data, decreases as a function of distance between transects (Fig. 7B, C). Assuming a linear decrease in similarity of sediment coverage patterns, 1.88 m is the distance that corresponds to zero similarity in flow coverage patterns on the shelf (Fig. 7B) and 3.17 m corresponds to zero similarity in flow coverage on the slope. In this experiment, the subaqueous advection-settling segment of the transport system propagated signals ~50% farther than the traction dominated subaerial segment.

Observations from the scatter plots in Figure 7 may be summarized as follows:

(a) Flow in the terrestrial or shallow water portion of the experiment was more dynamic than on the submarine slope.

(b) Flow coverage on the delta top correlated inversely with flow coverage on the slope.

(c) Flow patterns remained similar over longer distances within the submarine slope transport system relative to the shelf system.

<u>e. The topographic evolution of the continental slope</u>

We used SONAR data acquired every 10 minutes of experimental time at transects at 2.5 m, 3 m, 3.5 m, 4 m, and 4.5 m from the inlet to characterize topography and deposition on subaqueous slope surface through time (Fig. 8, A-I). The data, calculations and metrics used were as follows:

(a) **Cross-stream topography** (Fig. 8A)**:** Raw SONAR data, acquired at a horizontal resolution of 4mm and a vertical resolution of 1mm. Erroneous data (spikes) comprised less than 1% of total topographic data collected; they were deleted manually and replaced by the average of elevation measurements from the preceding and subsequent time steps. Each time-step at all transects was then smoothed using a moving average window of 10mm.

(2) **Mean elevation** (Fig. 8B): The mean elevation of the sub-aqueous surface above the initial experimental surface was calculated at every ten-minute increment in experimental run-time from the topographic profiles in Figure 8A as follows:

$$Z_{mean\ (t)} = \Sigma\ Z_{y(t)} / n$$

Where $Z_{y(t)}$ is the elevation at cross-stream position y at time t, $Z_{mean\ (t)}$ is the mean elevation of the transect at each time step t, and n is the total number of elevation measurements along each transect.

(3) **Mean elevation difference** (Fig. 8C): Elevation difference ($H_{y\ (t)}$) associated with each 10-minute time-step t was calculated at every point y along each transect by subtracting the previous elevation of the surface $Z_{y(t-1)}$ from the elevation of the current surface $Z_{y(t)}$, as in:

$$H_{y\ (t)} = Z_{y(t)} - Z_{y(t-1)}$$

The calculated elevation differences were then averaged to generate the mean elevation difference $H_{mean\ (t)}$ at every time step as in:

$$H_{mean\ (t)} = \Sigma(H_{y\ (t)})\ /\ n$$

(3) **Shape (curvature) of the depositional surface** (Fig. 8D): The cross-stream curvature of the experimental surface was calculated using the second derivative of elevation ($d^2Z_{y(t)}/dy^2$). Figure 8D shows the temporal evolution of divergent (convex-upward) and convergent (concave-upward) topography through time.

(4) **Cross-stream variance in surface elevation** (Fig. 8E): Variance ($S_{z\ (t)}$) in the measured elevation (Z_y) of the topographic surface was calculated as in:

$$(S_{Z\ (t)})^2 = \Sigma(Z_{y\ (t)} - Z_{mean\ (t)})^2 / (n-1)$$

(5) **Cross-stream variance in elevation difference** (Fig. 8F): Variance ($Sh_{(t)}$) in the measured elevation difference ($H_{y\ (t)}$) of the topographic surface was calculated as in:

$$(S_{H\ (t)})^2 = \Sigma(H_{y\ (t)} - H_{mean\ (t)})^2 / (n-1)$$

(6) **Cross-stream sediment coverage** (Fig. 8G): The fraction of the transect at which deposition occurred at each time-step was calculated by integrating the number of points where $H_{y\ (t)} \leq 0$, and dividing the result by the total number of measurements n.

(7) **Cross-stream discontinuity in sedimentation** (Fig. 8H): At every time-step, all points at which $H_{y\ (t)} > 0$ transition laterally to $H_{y\ (t)} \leq 0$ were totaled as a relative measure of lateral discontinuity in sedimentation.

(8) **Power spectral densities of topographic profiles through time** (Fig.9A): We analyzed the power spectral density (PSD) of cross-stream slope topography to characterize changes in the spatial scales associated with depositional elements on the slope as the delta prograded towards the shelf edge.

No erosion occurred on the slope. In the early stages of the experiment, very low deposition rates characterized all slope transects (Fig. 8 A-C). When a delta front mouth bar prograded past the shelf edge between Hours 12 and 14 (Fig. 3, 4A, 4B), all slope transects recorded an increase in deposition rate (Fig. 8B). The change in deposition rate was most pronounced at the two most proximal transects (Fig. 8B, 2.5 m and 3 m), where the prograding front of the deltaic mouth bars were constructed by rapid suspended sediment fallout from plunging plumes (Hour 14 in Fig. 3, 4A, 4B). A slight decrease in deposition rate was recorded at 2.5 m and 3 m after experiment Hour 14 (Fig. 8B), related to the progradation of the steeper delta front upstream of the mouth bar lobes.

At all slope locations, low sedimentation rates were associated with the gradual growth of subtle, linear depositional topography along streamwise paths that were persistently occupied by flow (Fig. 6A, 8A). Linear flow-parallel deposition displayed widths on the order of a few tens of centimeters while deposition rates were small before the delta arrived at the shelf edge (Fig. 4B, 8 A- D). At 4 m and 4.5 m from the inlet, these depositional ridges gradually grew and coalesced to form features that were tens of cm wide (Fig. 8A-D); the same change occurred more rapidly at 3.5 m, when sedimentation rates increased after the delta reached the shelf edge at Experiment Hour 14. Concomitant with increasing ridge widths, the transects at 3.5 m, 4 m, and 4.5 m all displayed increases in the fraction of the experimental surface that received sediment (Fig. 8G) and increases in the lateral continuity of sedimentation (Fig. 8H). Topographic features at 3.5 m, 4 m and 4.5 m were remarkably persistent for the experiment duration (Fig. 8D). Cross-stream variance in elevation and variance in deposit thickness increased gradually at all three transects after the delta arrived at the shelf edge at Hour 14, with the rates of increase more pronounced closer to the source (Fig. 8E, F).

Once the delta arrived at the shelf edge, the feeder channel stayed in place for almost two hours and constructed a protruding shoreline and large delta-front mouth bar (Fig. 3, Hours 12 - 14). Until Hour 13, the proximal transects at 2.5 m and 3 m from the inlet displayed gradual increases in the fraction of the experimental surface that received sediment, and in the lateral continuity of sediment beds, while maintaining low variance in deposit thickness (Fig. 8 F-H). With the arrival of the delta at the shelf edge, these transects displayed more uniformity in sediment coverage and continuity, and greater variance in deposit thickness (Fig. 8F-H). Rapid sedimentation at 2.5 m and 3 m from the inlet during this time (Fig.

8A-C) was concomitant with an abrupt reorganization in cross-stream curvature of the surface (Fig. 8D) and temporary increases in topographic roughness (Fig. 8E) and variance in deposit thickness (Fig. 8F).

Between Hours 14 and 20, flow was partitioned through multiple smaller channels and sheet flow on the delta top, and flow and sediment was lost off the edges of the ramp (Fig. 2, 3B, 5B-D). Flow expansion into sheets promoted sediment storage on the delta top, where it compensated for the prior period of base-level rise, and extended phase of channelization and sediment release (*sensu* Powell et al., 2012; Kim et al., 2014) during Hours 12-14. Local deposition rates decreased at 2.5 m and 3 m from the inlet as delta-top channels swept across the experimental surface. At these locations Hours 14 – 22 were characterized by smoothing of topography (Fig. 8E) and decreased variance of depositional thickness (Fig. 8F). When flow and sedimentation was primarily directed to more central locations, through a smaller number of channels, between Hours 22 and 26 (Fig. 2, 3), the same transects displayed a roughening of topography (Fig. 8E) and increase in the spatial variance in deposition rate/thickness (Fig. 8F). The persistence of topographic features decreased after Hour 14, and rapidly growing depositional topography at the fronts of deltaic channels moved around to different locations across the transect (Fig. 8A, D).

The power spectral densities (PSDs; Fig. 9) of topographic transects at 2.5 m, 3 m, 3.5 m, 4 m, and 4.5 m from the inlet all exhibited slight changes in the amplitude of topographic features across all wavelengths (e.g., ripples, flow-parallel linear depositional topography). Temporal changes in amplitude across wavelengths were greatest at 2.5 m, 3 m and 3.5 m from the inlet. The slopes of the PSDs at 3.5 m, 4 m, and 4.5 m remained broadly consistent through time and space (Fig. 9); however, transects at 2.5 m and 3 m displayed fluctuations in PSD slope through time. At these locations, wavelengths between 10mm and 50mm displayed the greatest variability in amplitude through time.

The topographic evolution of the continental slope can be summarized as follows:

(a) As the delta built out towards the shelf edge, small depositional rates on the slope produced slowly-growing, small wavelength (<10^2 cm), depositional topography that remained temporally persistent, and displayed low variance in sedimentation rate.

(b) Once the delta reached the shelf edge, the proximal parts of the continental slope were characterized by dynamic depositional topography, with large cross-stream wavelengths (>10^2 cm), and high variance in sedimentation rates.

(c) Sediment coverage increased gradually through time on the continental slope. At distal slope locations, lateral discontinuity in sedimentation increased gradually through time; on the proximal slope, an abrupt reduction in lateral discontinuity occurred when the delta arrived at the shelf edge.

f. Comparing proximal-to-distal depositional patterns on the slope

We assessed the similarity between patterns of sedimentation on the proximal and distal slope (Fig. 10 A, B). To do this, we first detrended the sediment coverage and sediment discontinuity data at each transect in Figures 8 E and F. We then plotted the detrended sediment coverage (Fig. 10A) and detrended sediment discontinuity data (Fig. 10B) associated with every time-step at each transect against the same data at every transect downstream of it.

Downstream similarities in sedimentation patterns on the slope (Fig.10 A, B) are comparable to downstream similarities in the flow occupation patterns on the slope (Fig. 7). The positive slope in cross-plots from different transects decreases with increasing distance apart (Fig. 10 A – D). Within the plotted data, we observed temporally discrete subsets that show variability in the slope of the cross-plotted data through time.

Similarity in sediment coverage, indicated by the positive linear slope of the cross-plotted data, decreases as a function of distance between transects. Assuming a linear decrease in similarity of sediment coverage patterns, 3.81 m is the distance that corresponds to zero similarity in sediment coverage patterns. Similarity in sediment discontinuity patterns also decreases as a function of distance between locations, with zero similarity projected to occur at 2.47 m on the advection-settling dominated.

4. Discussion

The results of this work are most relevant to short time-scales ($<10^3$ years), and shelf margins fed by rivers with sufficiently large sediment loads to generate hyperpycnal plumes (e.g., Huanghe river, China, Wright et al., 1990; Salinas River, California, U. S. A., Johnson et al., 2001; Fiumara creeks, Italy, Casalbore et al., 2011). In the current work, we framed our exploration of terrestrial-marine linkages on shelf margins around 3 central questions.

(1) Are delta channel dynamics reflected in flow and sedimentation on the continental slope?

In this experiment, the degree of channelization and the number of active channels on the delta top influenced the organization of flow on the slope. The 2-D flume experiments of Lamb et al., (2009) showed that river discharge, basin depth and bed slope all impact hyperpycnal plume plunge dynamics and the production of turbidity currents. Increases in discharge push the plunge point farther basinward, deeper basins increase the likelihood of plume collapse and turbidity current generation, and steeper bed slopes support the generation of self-accelerating turbidity currents (Lamb and Mohrig, 2009; Lamb et al., 2010). Our experiments offer insight into how network dynamics may influence hyperpycnal plume dynamics, flow and marine sedimentation.

Channelized delta-top flow was associated with less storage of sediment on the delta top. This configuration conserved sediment concentrations as well as flow velocity in the plumes that travelled beyond the shoreline; they funneled discharge past the shoreline through a narrower cross-section and facilitated the formation of thicker turbidity currents on the slope (Lamb et al., 2009). Thicker currents, less susceptible to frictional drag from the bed and ambient fluid, moved faster and maintained greater lateral continuity. They delivered thicker plume deposits and turbidite deposits to the continental shelf and/or slope.

Conversely, sheet flow increased sediment storage on the delta-top, reducing sediment concentrations and flow velocity at the mouths of deltaic channels. Delta front plumes spread over a wider area and resulted in thin turbidity currents on the slope. To conserve flow cross-sectional area and overcome frictional drag from the bed and ambient fluid, density currents collapsed into narrow lanes of flow characterized by roll waves (Balmforth and Mandre 2004). Sheet flow on the delta and shelf resulted in discrete, “lanes” of flow on slope; channelized flow on the shelf resulted in sheet flow on the slope. Thus, flow patterns at distal slope locations displayed an inverse relationship to flow patterns on the shelf (Fig. 7A, B).

These results suggest that signals of delta channel network reorganization and flow partitioning through delta top channels can propagate well past the shelf edge and into deep marine environments in cases where depositional hyperpycnal flows build a significant component of the continental shelf and slope (Fig. 7, A - C). At field scales, this implies that terrestrial environmental signals contained in flow and sediment are mostly effectively transferred to deep marine environments during phases when flow is contained within fewer deltaic channels.

Humans have occupied river floodplains and deltas for millennia, e.g., Mississippi delta (Mehta and Chamberlain, 2019), Rhine-Meuse delta (Pliny the Elder, 79; Roymans, 2000), Indus river (Kenoyer, 1991), for millennia, substantially modifying channel networks for flood control (Colten, 2018), navigation (McCall, 1984) and agriculture (Rehder,1999) in coastal regions. Fundamentally altered connections between rivers and floodplains (Colten, 2018) have inhibited sediment storage on floodplains, conserved flow discharge and sediment concentrations within a small number of channels.

Experimental results presented herein imply that, where rivers can generate hyperpycnal plumes, anthropogenic alterations to coastal regions have likely increased the efficiency of signal transfer to the deep ocean. This is of particular importance where industrial-scale agriculture in the river basins deliver large volumes of dissolved pollutants to the rivers they feed (Hiatt and Passalacqua, 2017; Passalacqua, 2017; Wohl et al, 2019). Although we do not here explore the role of submarine channel development (e.g., Yu et al., 2006; Sylvester et al., 2010; Cantelli et al., 2011; Fernandes et al., 2016; Fernandes et al., 2020), a number of compelling recent studies (e.g., Hughes Clarke 2016; Azpiroz-Zabala et al., 2017; Hage et al., 2019) highlight the importance of these conduits in transferring or recording terrestrial environmental information (e.g., dissolved or particulate pollutants, dissolved or particulate carbon) to the deep ocean.

(2) How effectively do shelf and slope systems transfer information from upstream?

Sediment transport in this experiment occurred through a mixture of suspension and traction. Deltaic depositional patterns were characteristic of traction-dominated, transport-limited systems (Johnson and Whipple, 2007; Whipple et al., 1998). On the other hand, sediment thicknesses on the slope, integrated in the cross-stream direction, displayed exponential downstream decay (Fig 4A - C) suggestive of advection settling (Lamb et al., 2009; Straub and Mohrig, 2006; Ganti et al., 2014).

On the shelf, bulk patterns in flow showed a decay in similarity over very short stream-wise distances (Fig 7B). This may be the results of fundamental differences in flow dynamics associated with (a) the streamwise spatial transition from deltaic channels to hyperpycnal plumes to turbidity currents, and/or (b) the temporal evolution at each transect from subaqueous shelf to subaerial delta, and/or (c) the dynamism of traction-dominated, subaerial deltaic deposition.

By contrast, the coverage and lateral continuity of flow and sedimentation in advection-settling dominated slope environments in this experiment were remarkably similar over longer distances for the duration of the experiments (Fig. 7C, Fig. 10 A-D). While similarity in flow and sedimentation can be expected to decrease with increasing distance between transects in both traction-dominated and advection-settling-dominated segments of shelf margin transport systems (Fig. 10, C-D), the length-scale over which similarity reduced to zero was shorter in traction dominated systems. Thus, upstream signals of flow organization propagated more effectively (over longer distances) within the submarine slope transport system relative to the shelf transport.

Our results support 2 key inferences:

(1) Terrestrial information, embedded in water chemistry or particulate matter, can propagate into deeper parts of the world's oceans when conveyed by advection-settling dominated, hyperpycnal-derived, turbidity currents. Decelerating turbidity currents fundamentally rely on the concentration of suspended sediment in the flow. Therefore, the critical factor that influences the distance over which information can be transferred from the terrestrial to submarine systems is the average distance that suspended particles travel in the flow, before deposition. This distance, termed the advection length, is equal to the width-averaged sediment flux divided by a particle's settling velocity (Lamb and Mohrig, 2009; Lamb et al., 2010; Ganti et al., 2014). This relationship between sediment advection lengths and the record of external environmental signals, was first proposed by Ganti et al. (2014), and is supported by our results.

(2) On data-limited continental slopes fed by depositional turbidity currents, sedimentation patterns from a few cross-stream transects may be used to forecast patterns at nearby transects with reasonable confidence. For example, the lateral variability in terrestrial environmental signals encoded in water chemistry and/or fully-suspended mineral, anthropogenic or organic sediment, are likely to be relatively similar over significant streamwise distances bounded by the characteristic advection length scale. By contrast, forecasting patterns at spatially distinct sites in deltaic environments is likely to be more challenging.

This information can therefore inform extrapolations of (a) modern/ancient particulate organic carbon burial rates in the deep ocean, (b) the spatial variability in terrestrial environmental signals in continent-derived marine sediment, and (c) ecological impacts of dissolved or particulate anthropogenic pollutants (Pohl et al. 2020; Kane and Clare 2019) that are delivered directly to deep marine benthic communities through hyperpycnal-derived, depositional turbidity currents.

(3) How does delta growth and progradation to the shelf edge impact sedimentation on the continental slope?

Our results suggest that the position of the delta on the shelf can have profound impacts on the partitioning of sediment on continental margins. Numerous previous studies have connected differences in shelf margin sedimentation patterns to delta position on the shelf (e.g., Sylvester et al., 2012; Swartz et al., 2016; Porebski and Steel, 2006; Covault et al., 2009). The experimental data presented here complements existing field-based theory and provides detail-rich kinematic insight into processes that are challenging to resolve at the field scale.

Sediment partitioning in this experiment was influenced by the base-level rise rate, due to which roughly 40% of the supplied sediment volume was stored on the delta top and the remaining ~60% of supplied sediment was fluxed beyond the shoreline and distributed between shelf and slope (Fig. 4D). The arrival of the delta shoreline at the shelf edge significantly enhanced sediment delivery to the slope, where most of the supplied sediment (~60%) was deposited. Thus, a marked increase in sedimentation rates on continental slopes can signal a delta's arrival at the shelf edge. Our results show that, under constant rates of sea-level rise, sediment-rich channels can drive autogenic progradation of deltas to the continental shelf edge, sustain the shoreline position at the shelf edge for extended periods of time and deliver significant fractions of their sediment loads to the deep ocean on millennial timescales. Our findings reinforce similar findings from field-scale data-sets (e.g., Carvajal et al., 2009; Steel et al., 2008; Carvajal and Steel, 2006), while resolving kinematic details that remain opaque from stratigraphic data-sets.

The enhanced delivery of sediment to the slope when the delta reached the shelf edge was connected to an abrupt reorganization in slope topography (Fig. 8) and lateral continuity of flow and sedimentation on the slope (Fig. 6 B, C). The progradation of the delta front mouth bars beyond the shelf edge produced a change from persistent and subtle depositional topography with small cross-stream wavelengths and low variance, to more dynamic sedimentation patterns and topography with larger cross-stream wavelengths and enhanced variance (Fig. 8, Fig. 9).

These results emphasize that the location of the delta with respect to the shelf edge can produce significant differences in the dynamics of sedimentation in hyperpycnal-dominated shelf margin settings, without changes in boundary conditions such as sea-level change rates and mass fluxes. Moreover, if characterized from acoustically imaged strata, these differences could potentially be used to reconstruct shoreline proximity in advection-settling-dominated regimes.

5. Conclusions

We used physical experiments to explore the impact of delta progradation on the linked dynamics of flow and sedimentation in terrestrial and submarine environments. We specifically focused on exploring the impact of shoreline position relative to the shelf edge on flow and sedimentation in subaerial and submarine environments. Our results illuminate rich, short timescale morphodynamics in linked terrestrial and submarine systems. Our results offer unique insight into the linkages between terrestrial and submarine transport systems; they apply to timescales that range from days to millennia, and to problems as diverse as nutrient and/or pollutant delivery to the deep ocean ecosystems and terrestrial paleoenvironmental reconstructions from marine sedimentary records.

The experimental results presented herein may be distilled into the following key findings:

(1) Patterns of flow and sedimentation on the slope are impacted by flow partitioning through delta-top channels and associated hyperpycnal plume dynamics. When channelized, delta-top flow was associated with higher localized water discharge and sediment concentrations; plunging hyperpycnal plumes created thick, fast-moving, and laterally continuous, turbidity currents on the slope. By contrast, sheet flow on the delta-top, produced thin, slow-moving and laterally discontinuous turbidity currents on the slope. From these patterns, we infer that terrestrial environmental signals are most effectively transferred to deep marine environments during phases when flow is contained within one or a few deltaic channels.

(2) The terrestrial to submarine boundary marked a transition in sedimentation styles from transport-limited to advection settling. Flow and sedimentation patterns displayed greater similarity over longer distances on the advection-settling-dominated subaqueous continental slope than on the transport-limited sub-aerial delta top. We may therefore infer that environmental signals carried by water and sediment in depositional turbidity currents can transfer environmental information over distances that scale with average advection lengths of fully suspended sediment.

(3) Delta progradation can play an important role in defining the scales of depositional topography and sedimentation dynamics on the slope. Before the delta arrived at the shelf edge, slow-growing, small wave-length depositional topography on the slope remained temporally persistent. These depositional elements had small cross-stream wavelengths associated with low variance in sedimentation; once the delta reached the shelf edge, the growth, progradation and lateral stacking of mouth bars on the proximal parts of the continental slope caused an abrupt switch to dynamic depositional topography with large cross-stream wavelengths and high variance in sedimentation.

Acknowledgements

This work was partially supported by Shell, The American Chemical Society Petroleum Research Fund, and the National Science Foundation (EAR-2029803). The authors thank Diana di Leonardo, Chris Esposito, Tushar Bishnoi and Qi Li for productive discussions and assistance in data collection for this work.

Figures and captions

Figure 1: a) A cross-sectional view of the experimental basin used. b) Sketch illustrating the 5 transition zones of flow from river to turbidity current, as well as locations of backwater point, shoreline, and plunge point (modified from Lamb & Mohrig, 2009).

a.

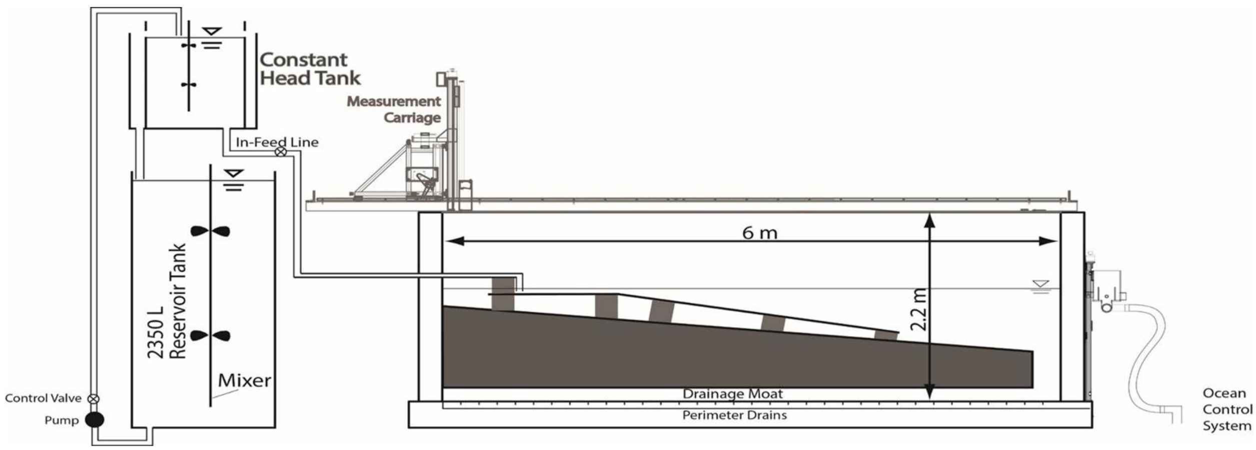

.

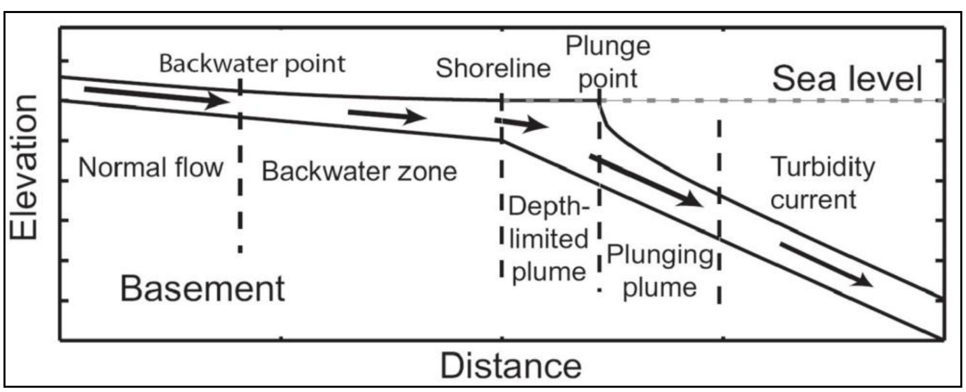

Figure 2: Overhead photographs were used to capture flow patterns on the shelf and slope.

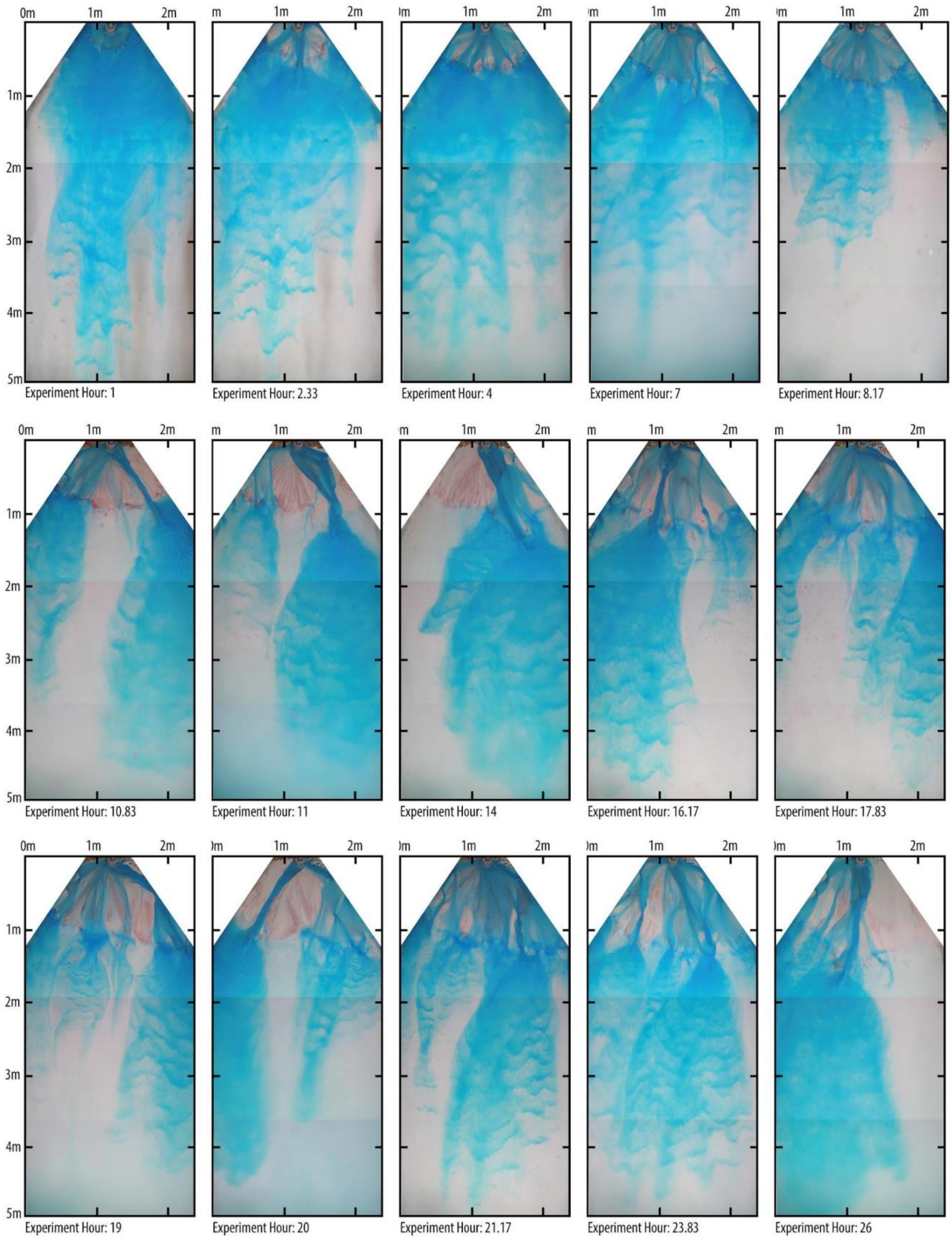

Figure 3: Time lapse maps of (a) elevation and (b) elevation change through the duration of the experiment.

a.

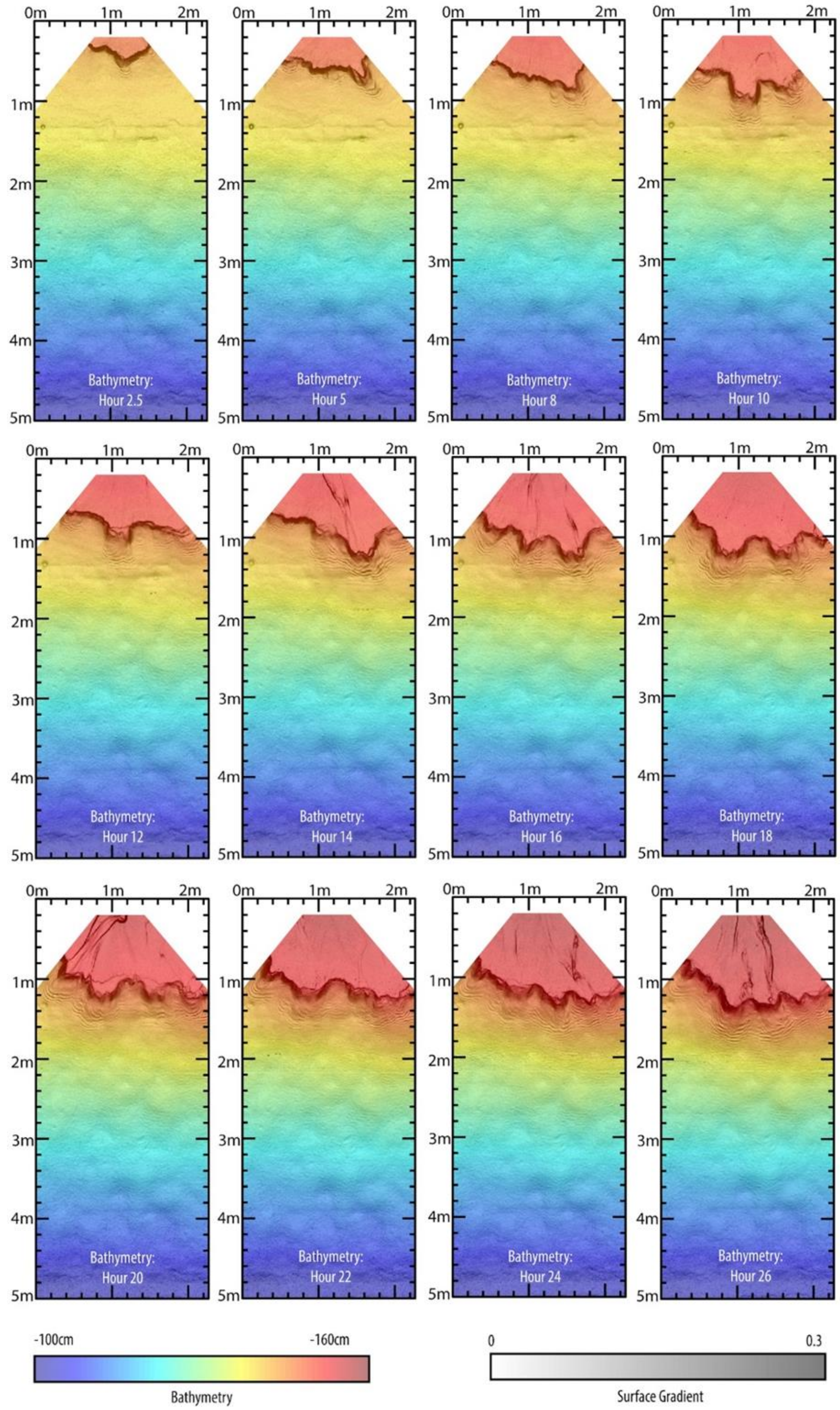

b.

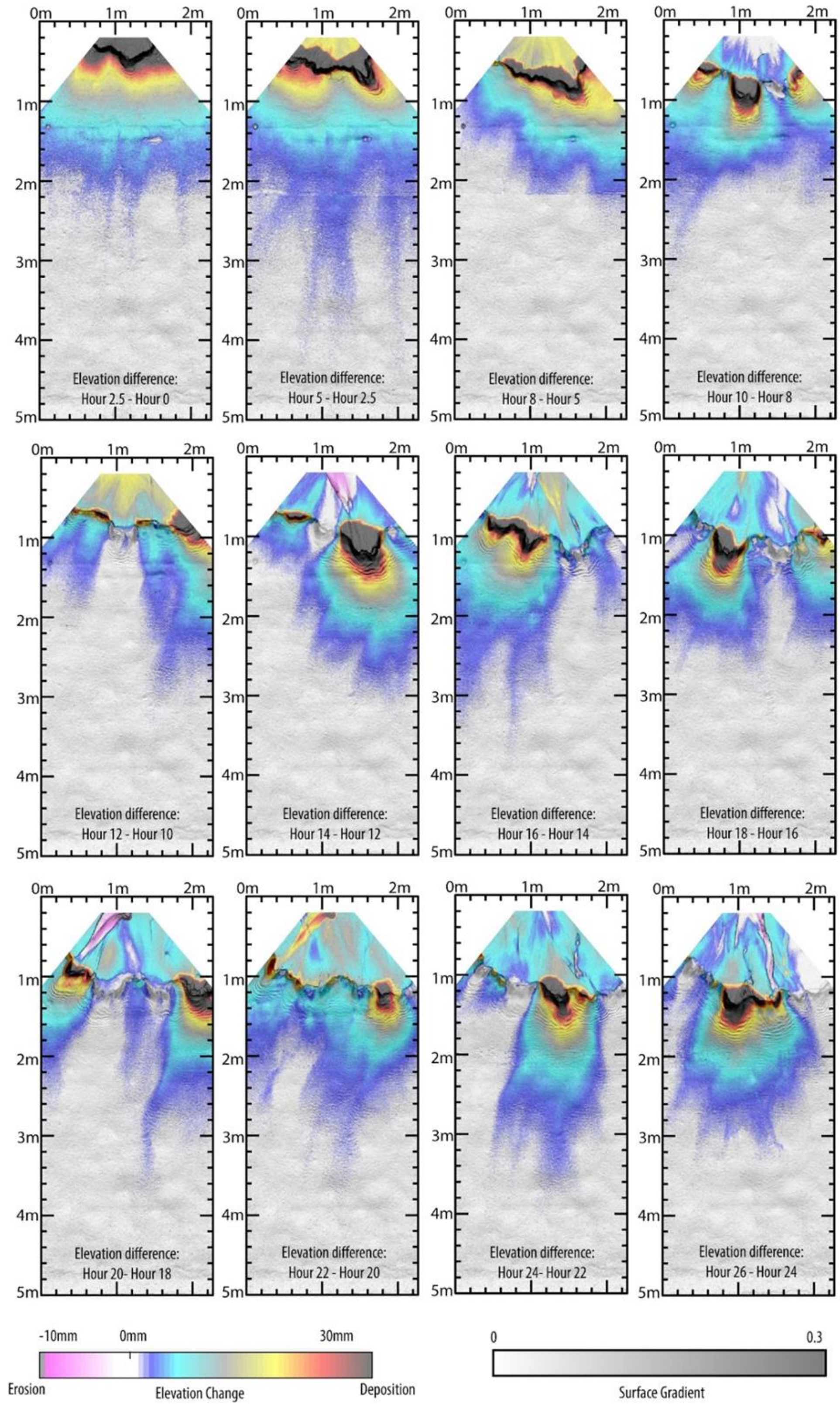
0m
1m
2m
3m
4m
5m
Elevation difference:
Hour 2.5 - Hour 0
Elevation difference:
Hour 5 - Hour 2.5
Elevation difference:
Hour 8 - Hour 5
Elevation difference:
Hour 10 - Hour 8
Elevation difference:
Hour 12 - Hour 10
Elevation difference:
Hour 14 - Hour 12
Elevation difference:
Hour 16 - Hour 14
Elevation difference:
Hour 18 - Hour 16
Elevation difference:
Hour 20- Hour 18
Elevation difference:
Hour 22 - Hour 20
Elevation difference:
Hour 24- Hour 22
Elevation difference:
Hour 26 - Hour 24
-10mm
0mm
30mm
Erosion
Elevation Change
Deposition
0
0.3
Surface Gradient

Figure 4: (a) A vertical dip-oriented slice through the preserved experimental stratigraphy. Note: the pinkish sediment is sand, the white sediment is silica flour. Location of the stratigraphic slice is shown on the (b) dip-oriented topographic transect through synthetic stratigraphy of the shelf and slope. At each 4mm increment in the stream-wise direction, we integrated cross-stream change in elevation to compute, (c) total volume deposited, (d) cumulative volume fraction of supplied sediment deposited (assuming 35% porosity) and (e) cumulative volume fraction of total sediment deposited.

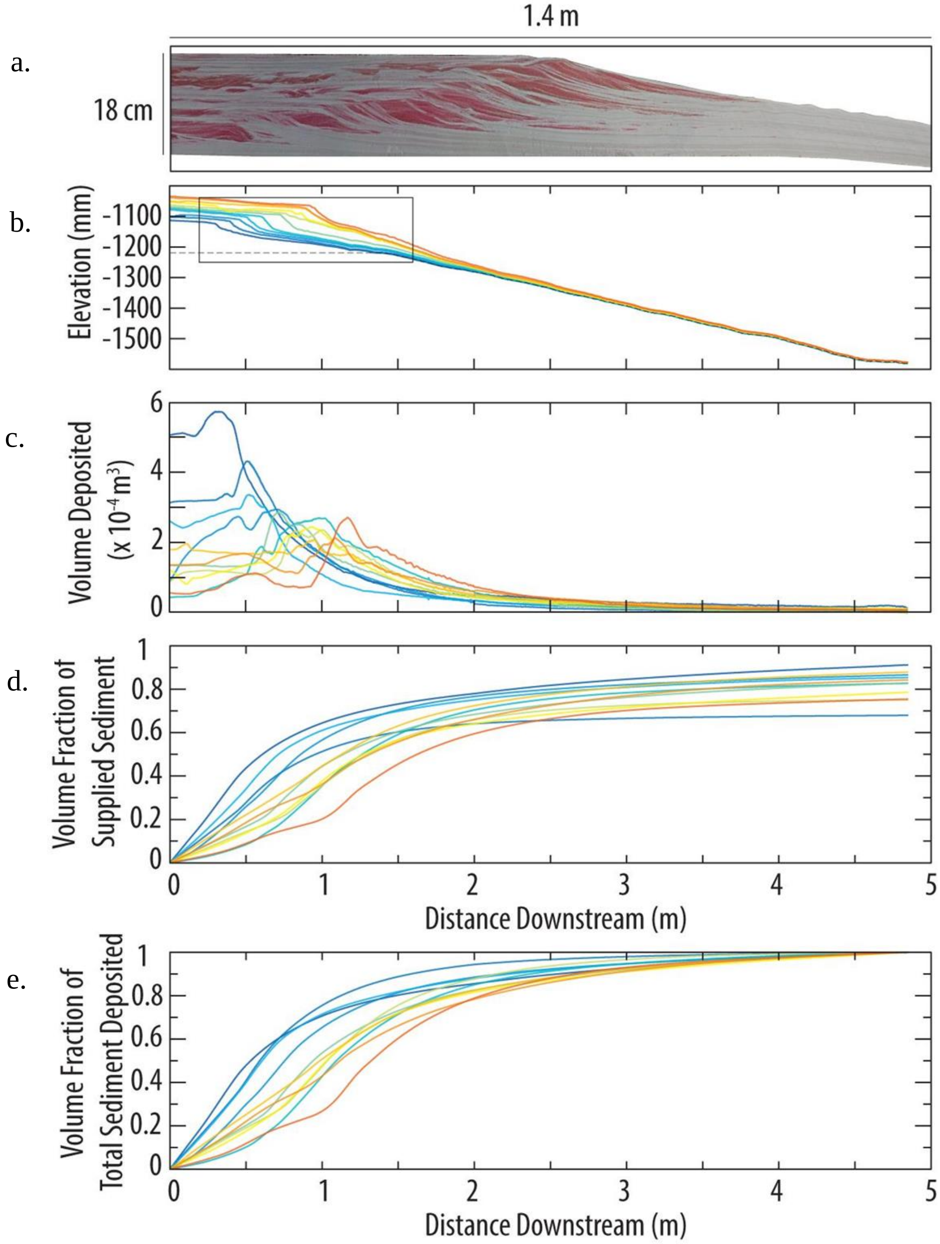

5. a.) Delta radius through time, measured from the inlet to every pixel along the shoreline. b.) Variance in delta radius through time. c.) Percent of delta surface inundated by flow on the expanding delta top through time. High values represent less channelized periods (sheet flow), low values represent more channelized periods. d.) Ratio of wetted area to dry area on the expanding delta-top.

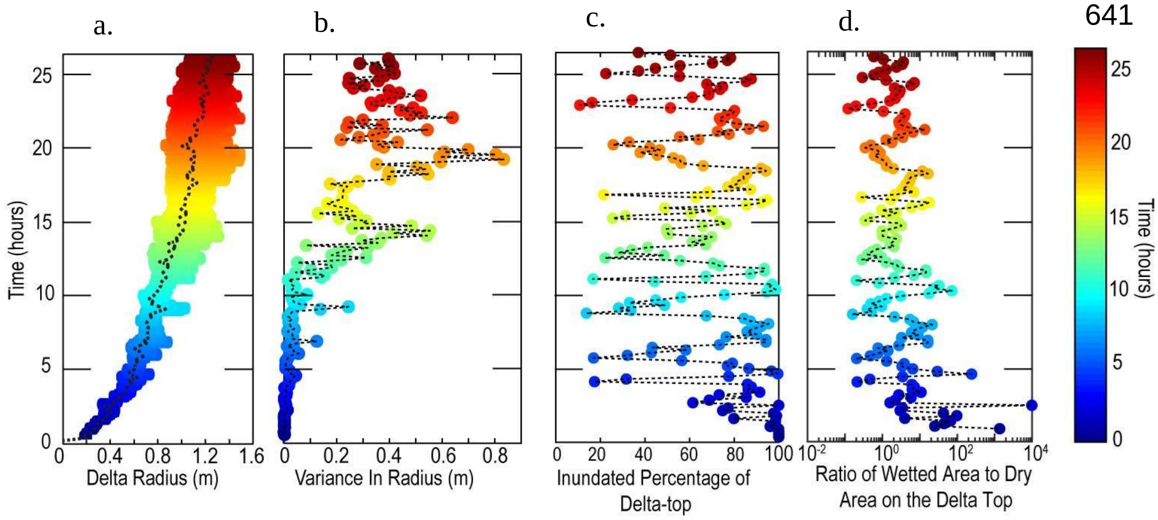

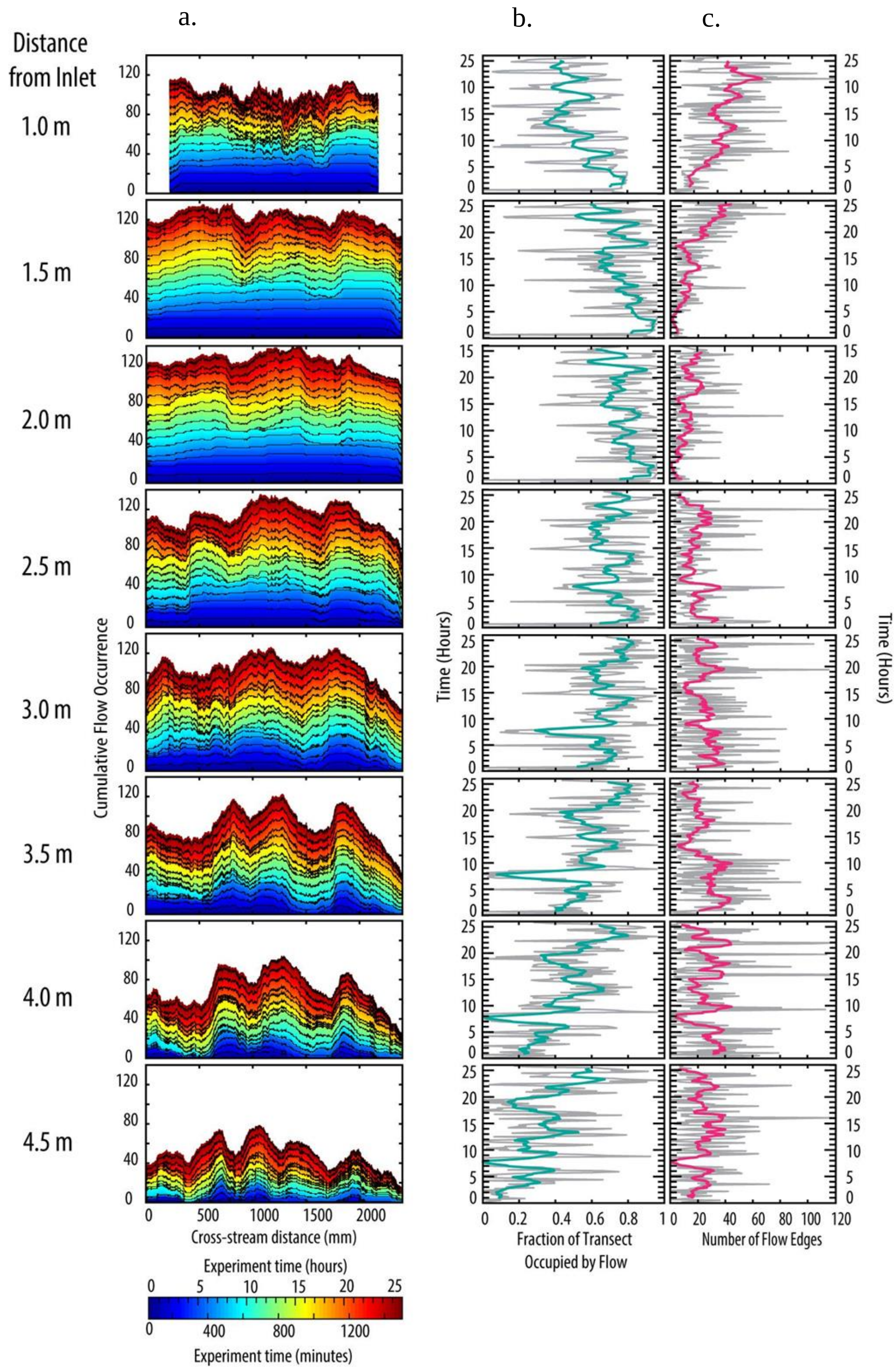

Figure 6: a.) The cumulative count of pixels with blue-dyed flow at each point along strike-oriented transects at 1.5, 2, 2.5, 3, 3.5, 4, 4.5 m from the inlet. The color bar is used to indicate time. Black lines are time-lines plotted every 100 minutes. Peaks indicate locations that were visited by subaerial flow or subaqueous turbidity currents most often. The difference between high and low values in these cumulative plots grows more pronounced from proximal to distal areas. b.) The fraction of the experimental surface covered by flow (calculated by summing up the number of blue pixels at every time step and dividing by the total width of the cross-section). The turquoise solid line shows the 2-hour moving average. High values indicate widespread, sheet flow on shelf and slope. On the shelf, low values indicate channelized flow; on the slope low values indicate the low flow coverage due to loss over the edges of the sloping ramp, or very localized flow. c.) The number of points identified at the boundaries of a zone of blue-dyed flow. The pink line shows the 2-hour moving average.

Figure 7: (a) Flow occupation patterns on the growing delta upstream compared to flow occupation patterns on the hyperpycnal plume-dominated slope downstream as a proxy for information transfer from shelf to slope. Each row of plots shows the de-trended flow occupation patterns at each transect, compared to every transect downstream of that location. The data points are color-coded to time-step. Similarity trends in flow coverage with distance between transects from (b) shelf to slope and (c) on the slope only.

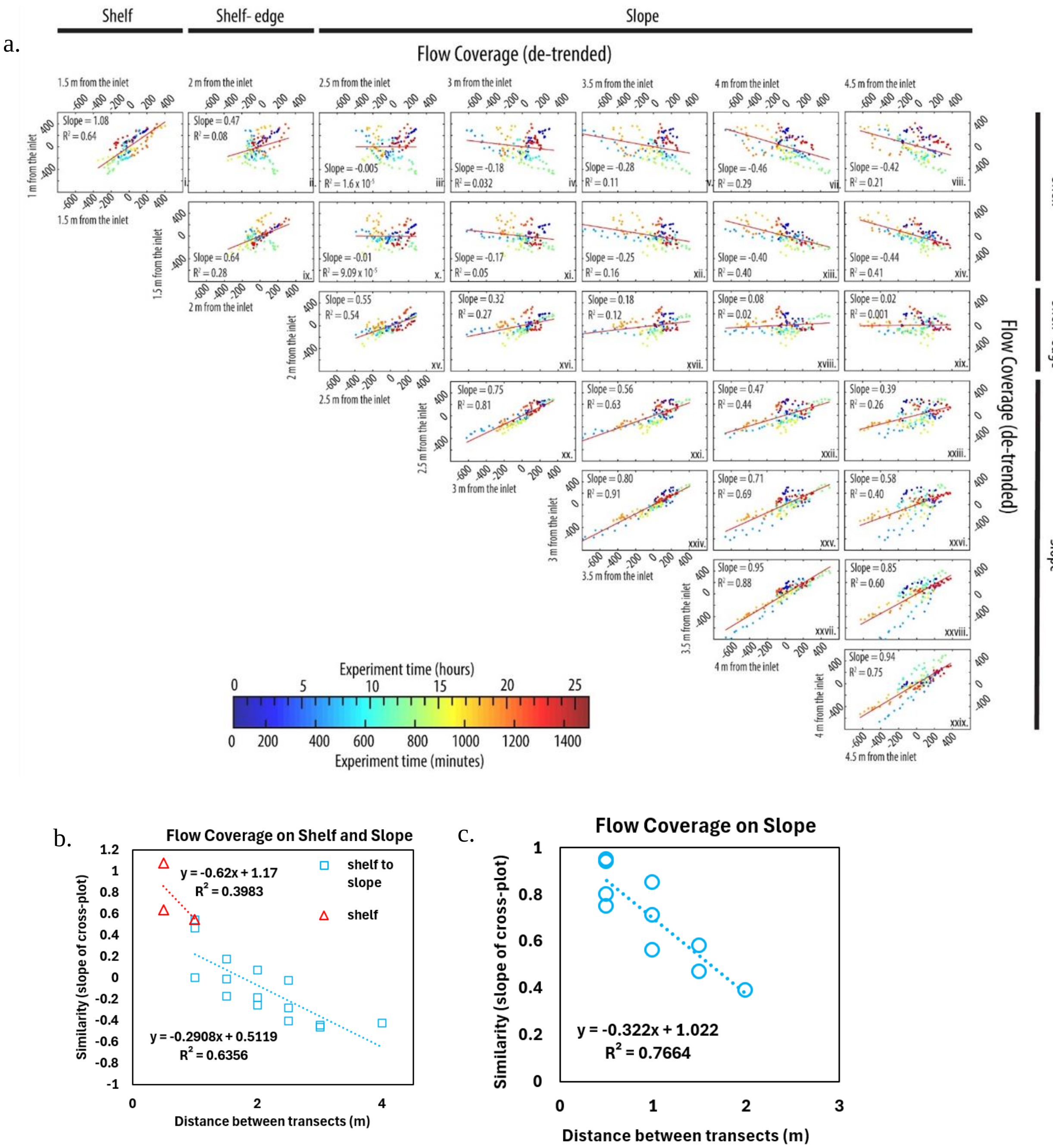

Figure 8: (a) Time-lapse topographic data, relative to the initial experimental surface along cross-stream transects at 2.5 m, 3 m, 3.5 m, 4 m, and 4.5 m from the inlet. The color bar is used to indicate time. Black lines are time-lines plotted every 100 minutes. At each transect, plots b through h show: (b) mean elevation gain through time, (c) mean deposit thickness through time, (d) the evolution of convergent and divergent depositional features through time, e) variance in elevation through time, (f) variance in deposit thickness through time, (g) the fraction of the transect that was covered by sediment, (h) lateral discontinuity in sedimentation through time, as measured by the number of sediment bed terminations.

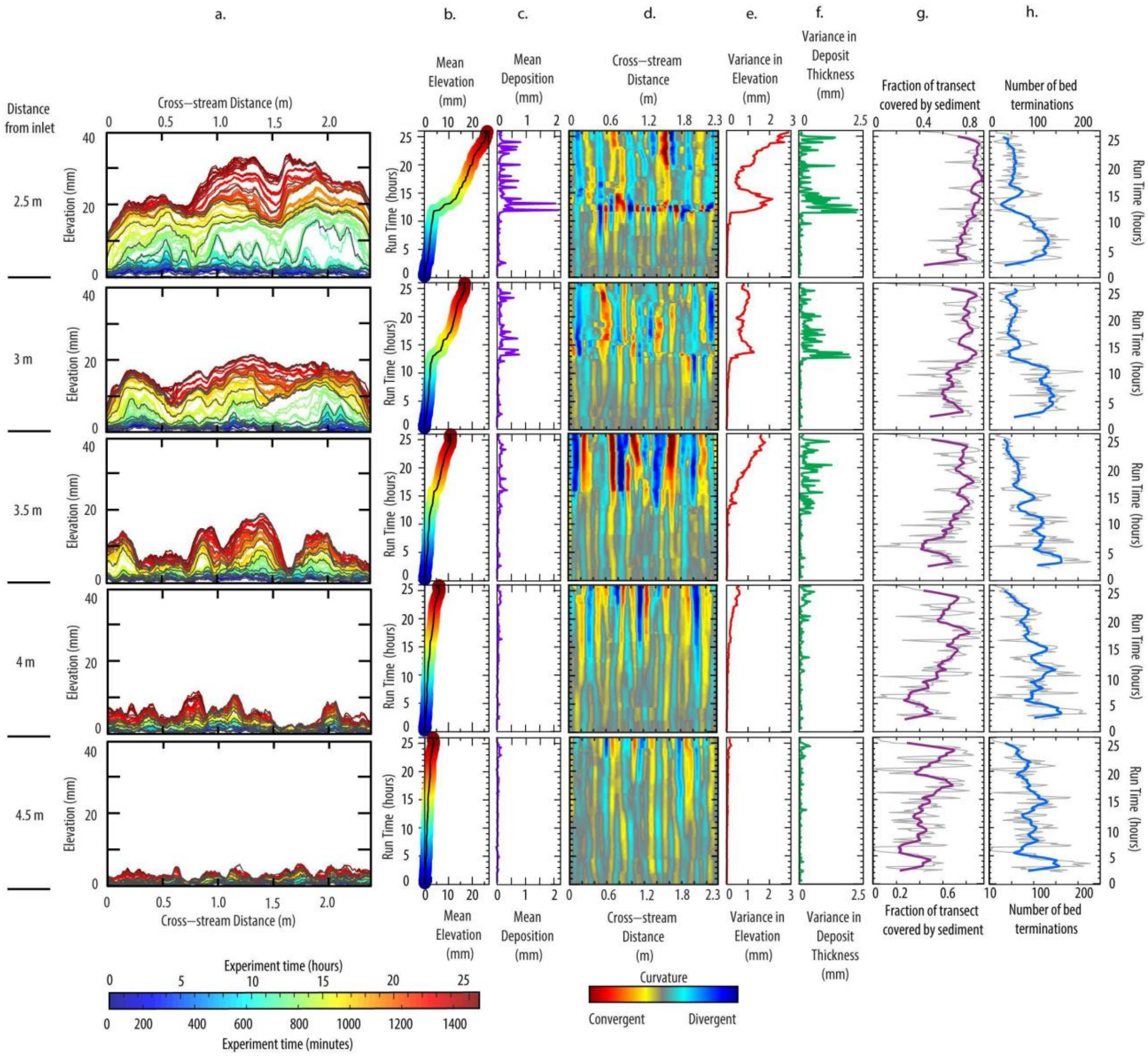

Figure 9: Power spectral densities of the sub-aqueous slope through time at (a) 2.5 m, (b) 3 m, (c) 3.5 m, (d) 4 m, and (e) 4.5 m from the inlet.

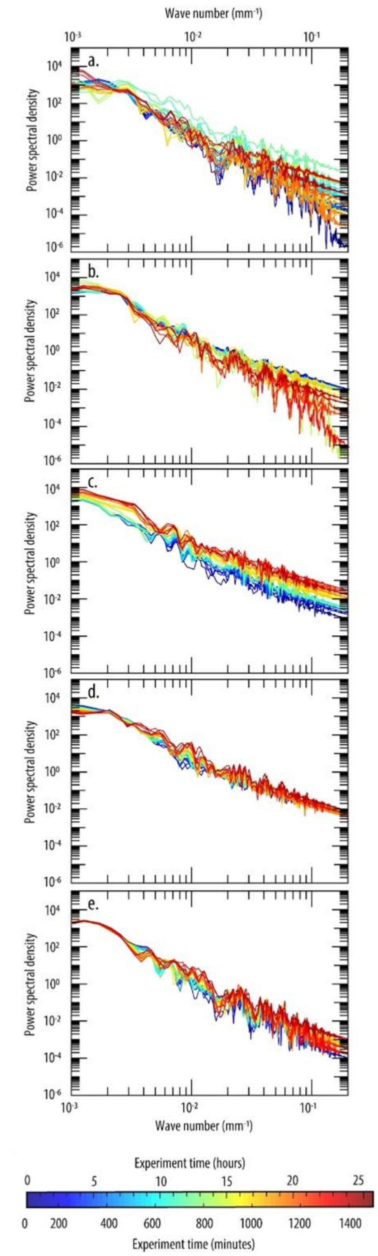

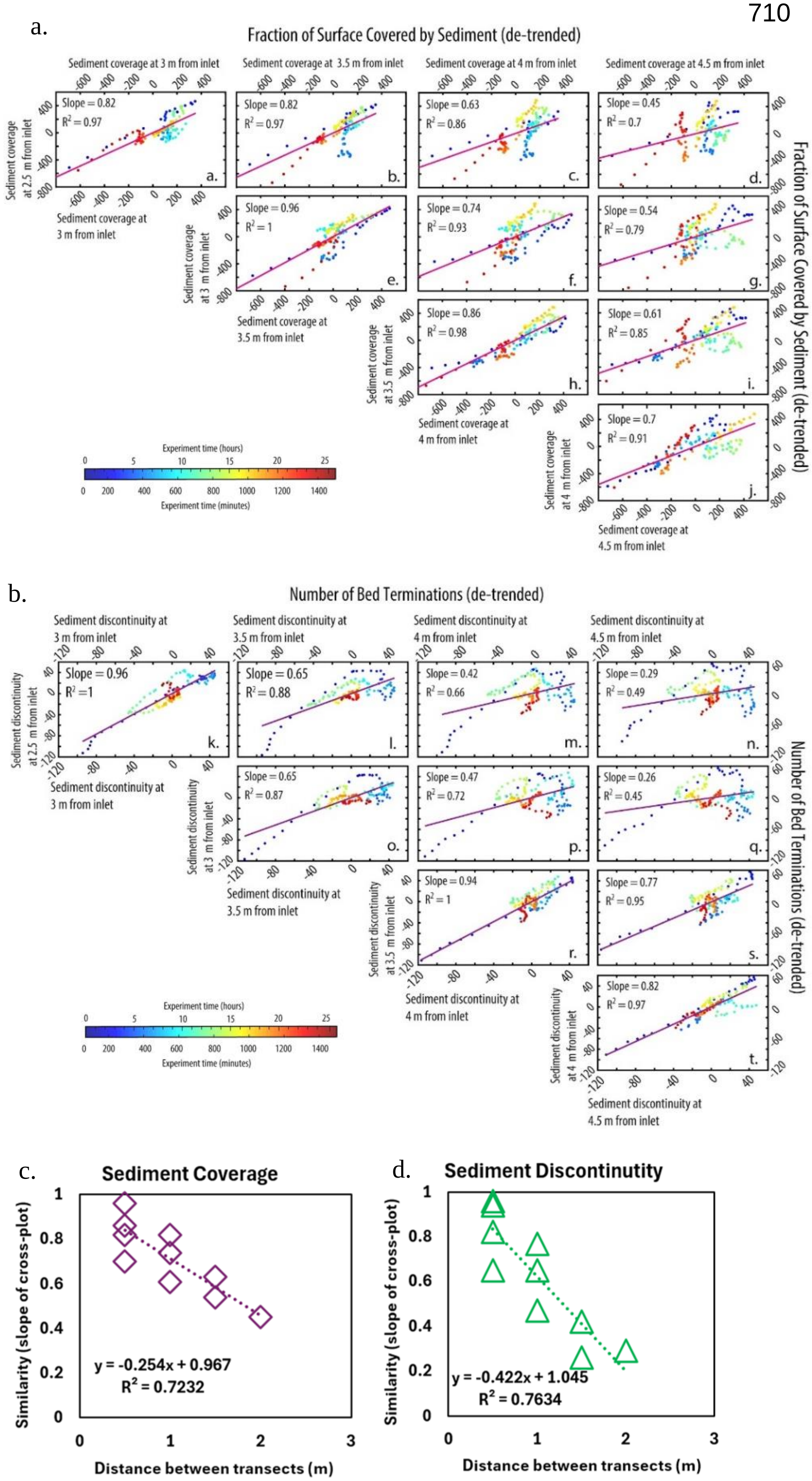

Figure 10: (a) The de-trended sediment coverage (from Fig. 8g) at each transect compared to the same at every transect downstream of that location. (b) The de-trended pattern of bed terminations at each transect, compared to every transect downstream of that location. The data points are color-coded to time-step. Similarity trends with in (c) sediment coverage, and (d) lateral discontinuity in sedimentation, on the slope with distance between transects.

References

Akiyama, J., and Stefan, H.G., 1984, Plunging flow into a reservoir—Theory: Journal of Hydraulic Engineering, v. 110, no. 4, p. 484–499.

AZPIROZ-ZABALA, M., CARTIGNY, M.J.B., SUMNER, E.J., CLARE, M.A., TALLING, P.J., PARSONS, D.R., AND COOPER, C., 2017a, A general model for the helical structure of geophysical flows in channel bends: Geophysical Research Letters, v. 44, p. 11,932–11,941, doi:10.1002/2017GL075721.

AZPIROZ-ZABALA, M., CARTIGNY, M.J.B., TALLING, P.J., PARSONS, D.R., SUMNER, E.J., CLARE, M.A., SIMMONS, S.M., COOPER, C., AND POPE, E.L., 2017b, Newly recognized turbidity current structure can explain prolonged flushing of submarine canyons: Science Advances, v. 3, no. e1700200, doi:10.1126/sciadv.1700200.

Balmforth, N. J., and S. Mandre. 2004. "Dynamics of Roll Waves." *Journal of Fluid Mechanics* 514 (September): 1–33.

Carvajal, Cristian R., and Ron J. Steel. 2006. "Thick Turbidite Successions from Supply-Dominated Shelves during Sea-Level Highstand." *Geology* 34 (8): 665–68.

Carvajal, Cristian, Ron Steel, and Andrew Petter. 2009. "Sediment Supply: The Main Driver of Shelf-Margin Growth." *Earth-Science Reviews* 96 (4): 221–48.

Casalbore, D., Chiocci, F.L., Scarascia Mugnozza, G. *et al.* Flash-flood hyperpycnal flows generating shallow-water landslides at Fiumara mouths in Western Messina Strait (Italy). *Mar Geophys Res* **32**, 257–271 (2011). https://doi.org/10.1007/s11001-011-9128-y

Chow, V.T., 1959, Open-Channel Hydraulics: New York, McGraw-Hill, 680 p.

Colten, C. E., 2018, Levees and the Making of a Dysfunctional Floodplain, In Mississippi Delta Restoration, J. W. Day, J. A. Erdman (eds), Estuaries of the Worls

Covault, Jacob A., Brian W. Romans, and Stephan A. Graham. 2009. "Outcrop Expression of a Continental-Margin-Scale Shelf edge Delta from the Cretaceous Magallanes Basin, Chile." *Journal of Sedimentary Research* 79 (7): 523–39.

Dixon, Joshua F., Ronald J. Steel, and Cornel Olariu. 2012. "River-Dominated, Shelf edge Deltas: Delivery of Sand across the Shelf Break in the Absence of Slope Incision." *Sedimentology* 59 (4): 1133–57.

Fernandes, A. M, Straub, K.M., Buttles, J., Mohrig, David, 2016, how do submarine channels form? An experimental perspective, Geological Society of America Abstracts with Programs. Vol. 48, No. 7 doi: 10.1130/abs/2016AM-286627

Fernandes, Anjali M., James Buttles, and David Mohrig. 2020. "Flow Substrate Interactions in Aggrading and Degrading Submarine Channels." *Journal of Sedimentary Research*. https://doi.org/10.2110/jsr.2020.31.

Fedele, Juan J., and Marcelo H. García. 2009. "Laboratory Experiments on the Formation of Subaqueous Depositional Gullies by Turbidity Currents." *Marine Geology* 258 (1): 48–59.

Ganti, Vamsi, Michael P. Lamb, and Brandon McElroy. 2014. "Quantitative Bounds on

Morphodynamics and Implications for Reading the Sedimentary Record." *Nature Communications* 5 (February): 3298.

Hage, Sophie, Matthieu J. B. Cartigny, Esther J. Sumner, Michael A. Clare, John E. Hughes Clarke, Peter J. Talling, D. Gwyn Lintern, et al. 2019. "Direct Monitoring Reveals Initiation of Turbidity Currents from Extremely Dilute River Plumes." *Geophysical Research Letters* 46 (20): 11310–20.

Harris, Ashley D., Jacob A. Covault, Sarah Baumgardner, Tao Sun, and Didier Granjeon. 2020. "Numerical Modeling of Icehouse and Greenhouse Sea-Level Changes on a Continental Margin: Sea-Level Modulation of Deltaic Avulsion Processes." *Marine and Petroleum Geology* 111 (January): 807–14.

Harris, Ashley D., Jacob A. Covault, Andrew S. Madof, Tao Sun, Zoltan Sylvester, and Didier Granjeon. 2016. "Three-Dimensional Numerical Modeling of Eustatic Control on Continental-Margin Sand distribution A. D. Harris et Al. Numerical Modeling of Eustatic Control on Continental-Margin Sand Distribution." *Journal of Sedimentary Research* 86 (12): 1434–43.

Henderson, F.M., 1966, Open channel flow: New York, Macmillan, 522 p.

Heller, P. L., Paola, C., Hwang, I., John, B., and Steel, R., 2001, Geomorphology and sequence stratigraphy due to slow and rapid base-level changes in an experimental subsiding basin (XES 96-1): AAPG Bulletin, v. 85, no. 5, p. 817-838.

Hiatt, M., and P. Passalacqua. 2015. "Hydrological Connectivity in River Deltas: The First-order Importance of Channel-island Exchange." *Water Resources Research*. https://agupubs.onlinelibrary.wiley.com/doi/abs/10.1002/2014wr016149.

Hoyal, D. C. J. D., and Sheets, B. A., 2009, Morphodynamic evolution of experimental cohesive deltas: Journal of Geophysical Research-Earth Surface, v. 114.

HUGHES CLARKE, J.E., 2016, First wide-angle view of channelized turbidity currents links migrating cyclic steps to flow characteristics: Nature Communications, v. 7, p. 11896, doi:10.1038/ncomms11896

Johnson, Joel P., and Kelin X. Whipple. 2007. "Feedbacks between Erosion and Sediment Transport in Experimental Bedrock Channels." *Earth Surface Processes and Landforms* 32 (7): 1048–62.

Kane, Ian A., and Michael A. Clare. 2019. "Dispersion, Accumulation, and the Ultimate Fate of Microplastics in Deep-Marine Environments: A Review and Future Directions." *Frontiers of Earth Science in China* 7. https://doi.org/10.3389/feart.2019.00080.

Kenoyer, Jonathan Mark (1991). "The Indus Valley tradition of Pakistan and Western India". *Journal of World Prehistory*. **5** (4): 164.

doi:10.1007/BF00978474. S2CID 41175522.

Khripounoff, A., Vangriesheim, A., Babonneau, N., Crassous, P., Dennielou, B., And Savoye, B., 2003, Direct observation of intense turbidity current activity in the Zaire submarine valley at 4000 m water depth: Marine Geology, v. 194, p. 151–158, doi:10.1016/S0025-3227(02)00677-1.

Kim, W., C. Paola, and J. B. Swenson.2300 n.d. "Shoreline Response to Autogenic Processes of

Sediment Storage and Release in the Fluvial System.” *Journal of Geophysical Research*. https://doi.org/10.1029/2006JF000470.

Kim, Yuri, Wonsuck Kim, Daekyo Cheong, Tetsuji Muto, and David R. Pyles. 2013. “Piping Coarse-Grained Sediment to a Deep Water Fan through a Shelf edge Delta Bypass Channel: Tank Experiments.” *Journal of Geophysical Research: Earth Surface* 118 (4): 2279–91.

Lamb, M. P., D. C. Mohrig, B. J. McElroy, B. Kopriva, and J. Shaw. 2009. “Reading River Response to Climate Change from Hyperpycnal-Plume Deposits.” In , 2009:U43A – 0061.

Li, Q., Yu., L., Straub, K.M. "Storage thresholds for relative sea level signals in the stratigraphic record" *Geology* , v.44 , 2016

Martin, J., Paola, C., Abreu, V., Neal, J., and Sheets, B., 2009, Sequence stratigraphy of experimental strata under known conditions of differential subsidence and variable base level: AAPG Bulletin, v. 93, no. 4, p. 503-533.

McCall, Edith S., 1984, Conquering the Rivers: Henry Miller Shreve and the Navigation of America's Inland Waterways (Louisiana State University, 1984). ISBN 0-8071-1127-9

Jayur Madhusudan Mehta & Elizabeth L. Chamberlain (2019) Mound Construction and Site Selection in the Lafourche Subdelta of the Mississippi River Delta, Louisiana, USA, The Journal of Island and Coastal Archaeology, 14:4, 453-478, DOI: 10.1080/15564894.2018.1458764

National Research Council, 2010, Landscapes on the edge: New horizons for research on Earth's surface: National Academy of Sciences.

National Research Council, 2012, New opportunities in the earth sciences: National Academy of Sciences.

Paola, C., Straub, K., Mohrig, D., and Reinhardt, L., 2009, The "unreasonable effectiveness" of stratigraphic and geomorphic experiments: Earth -Science Reviews, v. 97, p. 1-43.

Passalacqua, P. 2017. “The Delta Connectome: A Network-Based Framework for Studying Connectivity in River Deltas.” *Geomorphology* . https://www.sciencedirect.com/science/article/pii/S0169555X16301593.

Pliny the Elder, c.77, The Natural History

Pohl, Florian, Joris T. Eggenhuisen, Ian A. Kane, and Michael A. Clare. 2020. “Transport and Burial of Microplastics in Deep-Marine Sediments by Turbidity Currents.” *Environmental Science & Technology* 54 (7): 4180–89.

Porebski, S. J., and R. J. Steel. 2006. “Deltas and Sea-Level Change.” *Journal of Sedimentary Research* 76 (3): 390–403.

Powell, E. J., W. Kim, and T. Muto. n.d. “Varying Discharge Controls on Timescales of Autogenic Storage and Release Processes in Fluvio-deltaic Environments: Tank Experiments.” *Journal of Geophysical Research*. https://doi.org/10.1029/2011JF002097.

Rehder, JB, 1999, Delta Sugar: Louisiana’s vanishing plantation landscape. Johns Hopkins Uiniversity Press, Baltimore

Roymans, N., "The Lower Rhine *Triquetrum* Coinages and the Ethnogenesis of the Batavians", in: T. Grünewald & H.-J. Schalles (eds.), *Germania Inferior: Besiedlung, Gesellschaft und*

Wirtschaft an der Grenze der römisch-germanischen Welt (2000), 93–145, esp. 94.

Steel, Ronald J., Cristian Carvajal, Andrew L. Petter, and Carlos Uroza. 2008. “Shelf and Shelf-Margin Growth in Scenarios of Rising and Falling Sea Level,” January. https://doi.org/10.2110/pec.08.90.0047.

Straub, K. M., and D. C. Mohrig. 2006. “Morphodynamics of Levees Built by Turbidity Currents: Observations and Models.” In , 2006:OS23B – 1662.

Straub, K.M. and Wang, Y. "Influence of water and sediment supply on the long-term evolution of alluvial fans and deltas: Statistical characterization of basin-filling sedimentation patterns" *Journal of Geophysical Research ? Earth Surface* , 2013

Straub, Kyle M. 2019. “Morphodynamics and Stratigraphic Architecture of Shelf edge Deltas Subject to Constant vs. Dynamic Environmental Forcings: A Laboratory Study.” *Frontiers of Earth Science in China* 7. https://doi.org/10.3389/feart.2019.00121.

Swartz, J. M., D. C. Mohrig, S. P. S. Gulick, D. F. Stockli, M. S. Daniller-Varghese, and R. Fernandez. 2016. “Rapid Shut-off and Burial of Slope Channel-Levee Systems: New Imaging and Analysis of the Rio Grande Submarine Fan.” In , 2016:EP43B – 0958.

Swartz, John Marshall. 2019. *Channel Processes and Products in Subaerial and Submarine Environments Across the Gulf of Mexico*. University of Texas.

Sylvester, Zoltán, Mark E. Deptuck, Bradford E. Prather, Carlos Pirmez, and Ciaran O’byrne. 2012. “Seismic Stratigraphy of a Shelf edge Delta and Linked Submarine Channels in the Northeastern Gulf of Mexico,” January. https://doi.org/10.1016/j.marpetgeo.2010.05.012.

Wang, Y., Straub, K. M., and Hajek, E. A., 2011, Scale-dependent compensational stacking: An estimate of autogenic time scales in channelized sedimentary deposits: *Geology*, v. 39, no. 9, p. 811-814.

Whipple, Kelin X., Gary Parker, Chris Paola, and David Mohrig. 1998. “Channel Dynamics, Sediment Transport, and the Slope of Alluvial Fans: Experimental Study.” *The Journal of Geology* 106 (6): 677–94.

Wright, L.D., Wiseman, W.J., Yang, Z.S., Bornhold, B.D., Keller, G.H., Prior, D.B., and Suhayda, J.N., 1990, Processes of marine dispersal and deposition of suspended silts off the modern mouth of the Huanghe (Yellow River): Continental Shelf Research, v. 10, no. 1, p. 1–40,

Wright 2009 Wright, Rita P. (2009). The Ancient Indus: Urbanism, Economy, and Society. Cambridge University Press. ISBN 978-0-521-57219-4. Retrieved 29 September 2013.

Wohl, E., G. Brierley, and D. Cadol. 2019. “Connectivity as an Emergent Property of Geomorphic Systems.” *Earth Surface Processes and Landforms*. https://onlinelibrary.wiley.com/doi/abs/10.1002/esp.4434.

Xu, J.P., Barry, J.P., And Paull, C.K., 2013, Small-scale turbidity currents in a big submarine canyon: *Geology*, v. 41, p. 143–146, doi:10.1130/G33727.1.

Yu, B., Cantelli, A., Marr, J., Pirmez, C., O'Byrne, C., and Parker, G., 2006, Experiments on self-channelized subaqueous fans emplaced by turbidity currents and dilute mudflows: Journal of Sedimentary Research, v. 76, no. 6, p. 889-902.